The effect of ocean tide loading on the determination of earth rotation parameters

Rüdiger Haas and Hans-Georg Scherneck

Onsala Space Observatory (OSO), SE-439 92 Onsala, Sweden, (geo@oso.chalmers.se)

Abstract

One of the main reasons to do space geodetic observations for instance by using geodetic Very Long Baseline Interferometry (VLBI) is to acquire scientific data for earth rotation studies. The analysis of space geodetic observations requires completeness in the modeling of earth deformation effects. This includes as the largest contributions solid earth tides and ocean tide loading. We concentrate on the effect of modeling errors in ocean tide loading on the estimated earth rotation parameters. Particularly, neglecting the horizontal components of ocean tide loading perturbs the estimated earth rotation parameters on daily and subdaily time scale. Predictions and observations of this influence in the frequency and the time domain are compared and discussed in this paper for different geodetic VLBI networks.

1 Introduction

Geodynamic processes deforming the solid earth, displacing masses in the hydrosphere, atmosphere and the earth's core influence the earth's rotational behavior. One way to investigate these processes is to infer the driving mechanisms from studies of earth orientation variations. For this purpose space geodetic techniques like Very Long Baseline Interferometry (VLBI), Global Positioning System (GPS), Satellite Laser Ranging (SLR) and Lunar Laser Ranging (LLR) are used to measure earth rotation parameters.

In the analysis of space geodetic data all known earth deformation effects have to be accounted for. This includes the solid earth tides, and as the second largest effect ocean tide loading, on which we concentrate in this paper. Software packages for the analysis of geodetic VLBI data, e.g. CALC/SOLV/GLOBL [*Ma* et al., 1990], MODEST [*Sovers* and *Jacobs*, 1996], contain modules to compute ocean tide loading effects since many years. But software packages for other techniques, e.g. the Bernese analysis software for GPS data, only recently included this effect [*Rothacher*, 1998, pers. comm.].

Horizontal ocean tide loading displacements are smaller by a factor of 3 to 10 than the vertical ones but are of special importance for the study of polar motion and UT1 (PMU). Mismodeling of horizontal ocean tide loading in the analysis of space geodetic data introduces a common rotation of the network of space geodetic sites. The determined polar motion and UT1 parameters will be contaminated due to this mismodeling. We call this effect 'virtual PMU variations' (VPMU). These are mainly semidiurnal and diurnal oscillations since ocean tide loading occurs mainly in these frequency bands. The effects are especially important for sparse networks with a small number of participating stations. As the number of stations of the network increases, the common rotation mode becomes more and more rejected and will converge to zero in a continuum situation.

In our paper we predict virtual PMU variations in the frequency and the time domain for the worst case of a complete neglection of horizontal ocean tide loading and compare the predictions to results obtained from the analysis of geodetic VLBI data. We also show that differences in existing ocean tide loading models can introduce 'model dependent virtual PMU variations' (MD-VPMU) with significant magnitude. Regarding expectation of future measurement accuracy in particularly VLBI they appear to be significant.

2 Ocean tide loading

The earth's crust is affected by the load of oceanic masses which are redistributed by ocean tides. The crust deforms mainly elastically to this load and site displacement of several centimeters for the vertical and a tenth to a third of it for the horizontal component are induced. Ocean tides are coherent in frequency with the solid earth tides but due to the geometry of the oceanic basins and hydrodynamic resonance effects they show a complicated geographic distribution. So the resulting ocean tide loading effects are strongly site dependent.

Usually this complex hydrodynamic problem is parameterized in a site dependent ocean tide loading model, and a number of amplitude and phase parameters are determined for each site. The loading parameters are computed using tidal amplitudes and phases from ocean tide models and Green's functions. Usually the 11 most important tides are treated individually, and the others can optionally be interpolated on the basis of the admittance spectrum. We will concentrate in the following on the three ocean tide loading models by *Scherneck* [1991, 1996] which are based on the ocean tide models by *Schwiderski* [1980], *Le Provost* et al. [1994] and on the CSR3.0 ocean tide model [*Eanes* and *Bettadpur*, 1995] and will be called M-S, M-L and M-C, respectively.

Figure 1 shows radial ocean loading amplitudes for the M_2 tide in the Atlantic ocean area according to the ocean loading model M-L based on the ocean tide model by *Le Provost* et al. [1994]. Strong loading effects occur in western Europe, at the east coast of North American and the north-east coast of South America.

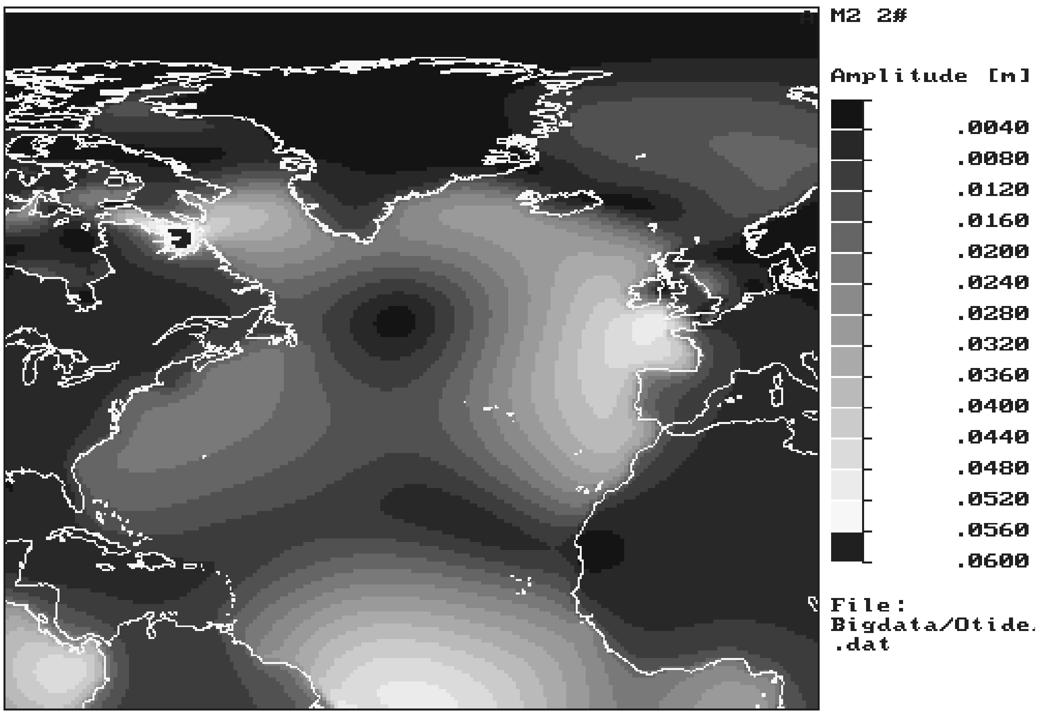

Fig. 1: Vertical ocean tidal loading for the M_2 tide according to the model M-L by *Scherneck* [1996] based on the ocean tide model by *Le Provost* et al. [1994]

Table 1 shows ocean tide loading amplitudes and phases of the strongest tide (M_2) for the VLBI stations Fortaleza (Brazil) and Westford (USA). The latter site on the north-east coast of the USA is frequently used in geodetic VLBI observations for Earth rotation studies. The inclusion of the Gulf of Maine in the ocean tide models is an importance difference between the three ocean tide loading models. The more recent ocean tide models by *Le Provost et al.* [1994] and *Eanes* and *Bettadpur* [1995] do not include this ocean basin which is strongly resonant near the M_2 tide frequency [*Greenberg*, 1987] while the older ocean tide model by *Schwiderski* [1980] does.

Tab. 1: Ocean tidal loading models for Fortaleza (Brazil) and Westford (USA): (u)p, (e)ast and (n)orth components, amplitudes A in [mm] and phases Φ in [°] for the M_2 tide. The models are: 1 Model M-S based on *Schwiderski* [1980], 2 Model M-L based on *Le Provost et al.* [1994], 3 Model M-C based on *Eanes and Bettadpur* [1995].

site	tide	component	M-S[1]		M-L[2]		M-C[3]	
			A [mm]	Φ [°]	A [mm]	Φ [°]	A [mm]	Φ [°]
Fortaleza	M_2	u	32.67	39.7	36.01	34.0	37.63	34.3
		e	3.13	28.8	4.69	16.4	4.97	20.8
		n	5.35	62.9	5.08	51.0	5.64	51.9
Westford	M_2	u	10.24	185.0	8.24	162.4	8.15	165.4
		e	4.21	215.2	2.58	212.0	2.75	208.3
		n	2.25	324.4	1.62	350.3	1.67	354.9

From the ocean tide loading models M-S, M-L and M-C maximum absolute effects of site displacement can be calculated which is shown in Table 2 for frequently used geodetic VLBI sites. For these stations the maximum peak displacements can reach 70 mm and 12 mm for the vertical and horizontal components, respectively.

Tab. 2: Maximal ocean tide loading effects (u)p, (e)ast and (n)orth in [mm] for frequently used geodetic VLBI sites. See Table 1 for description of the models.

VLBI site	M-S			M-L			M-C		
	u	e	n	u	e	n	u	e	n
Algonquin (Canada)	15.4	5.1	1.5	16.5	4.6	1.2	16.1	4.8	1.4
Fortaleza (Brazil)	61.4	7.0	11.2	67.8	9.1	11.3	70.5	9.6	11.9
Gilmore Creek (USA)	25.0	3.5	10.2	26.9	3.9	10.9	28.6	3.6	10.6
Green Bank (USA)	17.9	5.9	1.4	18.3	5.1	1.0	18.2	5.4	1.0
Hartebeesthoek (South Africa)	32.7	3.4	3.3	36.0	2.5	3.8	33.9	2.9	3.7
Hobart (Australia)	32.4	10.5	6.0	32.9	9.8	6.0	33.1	10.1	5.9
Kokee Park (USA)	41.6	9.5	11.0	43.4	9.5	11.5	48.3	9.8	11.9
Ny Ålesund (Norway)	21.4	5.9	4.2	23.5	5.8	5.1	24.1	6.1	5.2
Onsala (Sweden)	12.0	3.7	2.2	11.6	3.8	2.4	11.8	3.7	2.4
Westford (USA)	25.4	7.5	4.6	22.9	5.1	3.5	23.3	5.5	3.9
Wettzell (Germany)	12.0	3.7	2.2	11.6	3.8	2.4	11.8	3.7	2.4
Yellowknife (Canada)	17.3	7.3	3.9	18.7	7.6	4.1	19.5	7.5	3.7

3 Predicting virtual PMU variations

Two realizations of a space geodetic networks consisting of a finite set of observing stations give different results for polar motion and UT1 depending on how the horizontal ocean tide loading is modeled. The differences will be in the frequency spectrum of the ocean tide loading, so the largest effects are to be expected in the semidiurnal and diurnal frequency range. The worst case is the complete neglection of horizontal ocean tide loading while the second worse case is mismodeling of the horizontal ocean tide loading effects.

The effects can be predicted using usual Helmert transforms. We transform the amplitude and phases of horizontal ocean tide loading for the stations participating in a geodetic VLBI network into a common rotation of the network which can be described by three rotation angles corresponding to polar motion and UT1. So for each tide included in ocean tide models a set of three rotation angles can be derived. Usually 11 main tides are included in ocean tide loading models, so 11 times three rotation angles can be derived from the Helmert transforms. From this representation in the frequency domain it is easy to calculate time series of virtual PMU variations for any period of interest.

Table 3 shows as an example amplitudes of prograde and retrograde polar motion and amplitudes of UT1 for the NEOS-A network consisting of the five stations Fortaleza, Green Bank, Kokee Park, Ny Ålesund and Wettzell for the case that ocean tide loading according to model M-S based on the ocean tide model by Schwiderski [1980] is neglected completely. The amplitudes for virtual PMU variations reach values of 50 μas and 1.5 μsec, respectively.

Tab. 3: Frequency domain representation of virtual PMU variations for the NEOS-A geodetic VLBI network. Shown are amplitudes of polar motion (prograde and retrograde) in [μas] and UT1 variations in [μsec] due to the neglection of horizontal ocean tide loading according to model M-S.

	polar motion				UT1	
	prograde		retrograde			
tide	Ap_1	Ap_2	Ar_1	Ar_2	A_1	A_2
M_2	−10.3	24.9	−52.3	19.8	0.8	1.9
S_2	1.0	7.4	−19.3	−2.9	0.4	0.6
N_2	−4.0	5.1	−9.9	6.4	0.0	0.4
K_2	1.0	1.3	−4.8	−1.3	0.0	0.1
K_1	3.4	−10.7	−5.6	−8.3	−1.3	1.0
O_1	3.5	−5.1	−6.6	−2.2	−1.5	0.1
P_1	1.1	−3.3	−1.8	−2.4	−0.4	0.3
Q_1	0.7	−1.3	−1.7	−0.2	−0.3	−0.1
Mf	0.8	−1.4	1.6	−1.1	0.1	0.0
Mm	0.3	−0.7	0.5	−0.4	0.1	0.0
Ssa	0.3	0.2	1.2	−1.3	0.2	−0.1

In a similar way model dependent virtual PMU variations (MD-VPMU) can be calculated by Helmert transform. Here we transform the differences in the horizontal ocean tide loading according to the different models into virtual rotations.

Maximum effects for VPMU variations and MD-VPMU variations can be calculated and are shown in Table 4 for different geodetic VLBI networks used for earth rotation studies. The VLBI networks are IRIS-S (Fortaleza, Gilmore Creek, Hartebeesthoek, Westford, Wettzell), NEOS-A (Fortaleza, Green Bank, Kokee Park, Ny Ålesund, Wettzell), CORE-A (Algonquin, Gilmore Creek, Hartebeesthoek, Hobart, Matera, Westford) and CORE-B (Algonquin, Fortaleza, Gilmore Creek, Goldstone, Kashima, Onsala, Wettzell, Yellowknife). The values are maximum values for a time period of 20 years and assume ideal geometry and parameter estimation. The maximum values for VPMU reach 190 μas and 130 μas for x_p and y_p, respectively and 10 μsec for UT1, the maximum values for MD-VPMU reach 40 μas and 25 μas for x_p and y_p, respectively, and nearly 3 μsec for UT1. Since hourly estimates for polar motion and UT1 have formal errors of about 120 μas and 8μsec, respectively [*Gipson*, 1996], the predicted VPMU are within the resolving power of the observations. The MD-VPMU are small compared to the present day accuracies and so cannot be detected today. However the effects may exceed the detection threshold with the expected increase of accuracy in VLBI in the CORE program [*Clark* et al., 1997].

Tab. 4: Maximal VPMU and MD-VPMU variations due to the neglect or differences of horizontal ocean tide loading, respectively for different VLBI networks. Polar motion is given in [μas], UT1 in [μsec]. VPMU variations are calculated from neglect of 1 model M-S, 2 model M-L and 3 model M-C. MD-VPMU variations are calculated exchanging 4 model M-S and M-L, 5 model M-S and M-C and 6 model M-L and M-C. See text for the description of the VLBI networks.

Network		${V_S}^1$	${V_L}^2$	${V_C}^3$	${D_{SL}}^4$	${D_{SC}}^5$	${D_{LC}}^6$
IRIS-S	x_p	185.3	187.2	188.6	28.4	24.6	12.4
	y_p	67.9	66.7	71.2	11.2	12.1	11.3
	$UT1$	5.5	7.1	8.1	2.1	2.9	1.1
NEOS-A	x_p	110.8	114.8	123.7	23.2	29.5	11.8
	y_p	125.8	123.9	130.5	25.2	12.9	16.6
	$UT1$	6.8	7.0	7.7	2.5	2.4	0.8
CORE-A	x_p	116.7	103.9	96.8	40.2	35.7	11.7
	y_p	40.7	33.2	32.5	15.7	17.5	5.4
	$UT1$	5.3	6.3	6.3	1.6	1.3	0.6
CORE-B	x_p	135.4	135.0	131.4	32.2	25.4	16.2
	y_p	70.6	72.7	81.8	13.0	17.1	17.6
	$UT1$	8.3	9.7	9.9	2.0	2.0	0.7

4 Comparing predictions to results from VLBI analyses

In this chapter we describe the work we did concerning the comparison of predicted and observed VPMU variations. We concentrated on the worst case, the complete neglection of horizontal ocean tide loading. The comparisons were performed in the frequency and in the time domain.

For the comparison in the frequency domain we used the data of IRIS-S network. Since there has been some changes in the network configuration during the years we had to find a set of stations representing the IRIS-S network. We chose the four stations Fortaleza, Hartebeesthoek, Westford and Wettzell because they participated in most of the sessions. With this set of stations we predicted amplitudes of VPMU in the frequency domain according to M-S using Helmert transforms as described before.

We used the IRIS-S data set from 1986 to 1998 to derive high frequent polar motion and UT1 values at tidal frequencies. Radio source coordinates, station coordinates and velocities were fixed to the most recent global VLBI solution by Goddard Space Flight Center [*Ma* and *Ryan*, 1998] as well as polar motion UT1 and nutation. Clock and atmosphere parameters were estimated piecewise linearly for each session and high frequent polar motion and UT1 amplitudes as global parameters. We prepared two solutions, one applying horizontal and vertical ocean tide loading according to M-S and one applying only vertical ocean tide loading according to M-S. Then we calculated the differences of the results for the high frequency polar motion and UT1 amplitudes determined in these two solutions. Table 5 shows predictions and observations for virtual PMU variations due to neglection of horizontal ocean tide loading according to M-S for the 2 strongest tides in the semidiurnal and the diurnal frequency band for the IRIS-S network.

Tab. 5: Predicted and observed VPMU variations in the frequency domain for the two strongest tides in the semidiurnal and diurnal frequency band due to neglect of horizontal ocean tide loading according to model M-S for the IRIS-S network.

polar motion, prograde					polar motion, retrograde			
	predicted		observed		predicted		observed	
tide	Ap_1 [μas]	Ap_2 [μas]	Ap_1 [μas]	Ap_2 [μas]	Ar_1 [μas]	Ar_2 [μas]	Ar_1 [μas]	Ar_2 [μas]
M_2	-21.2	50.3	-3.8 ± 12.1	22.9 ± 12.0	-43.8	-20.9	-25.4 ± 12.2	-18.2 ± 12.3
S_2	2.7	13.3	5.6 ± 12.2	5.2 ± 11.6	-11.0	-14.8	-6.3 ± 12.4	-14.7 ± 11.8
K_1	8.9	4.5	-15.3 ± 14.0	-5.6 ± 14.9	-11.1	-8.5	-13.9 ± 14.1	19.9 ± 15.0
O_1	4.9	1.4	-6.0 ± 14.5	6.9 ± 14.3	-1.8	-2.8	-5.3 ± 14.5	-19.0 ± 14.6
UT1								
tide	A_1 [μsec]	A_2 [μsec]	A_1 [μsec]	A_2 [μsec]				
M_2	-1.6	1.6	-3.4 ± 1.2	-0.5 ± 1.2				
S_2	-0.7	0.6	-1.7 ± 1.2	-0.4 ± 1.1				
K_1	0.2	-0.1	0.2 ± 1.4	0.8 ± 1.4				
O_1	-0.2	-0.2	-1.5 ± 1.4	-0.3 ± 1.4				

The comparison in the frequency domain shows that the predicted effects can be verified to a large extent. The neglect of horizontal ocean tide loading introduces amplitudes of VPMU variations similar to the predicted values. The semidiurnal tides show a better agreement than the diurnal ones. However, the agreement is not perfect which should not be surprising since the predictions as based on idealized assumptions as to source geometry and independence of estimated parameters. This is not true in the real-world case. The IRIS-S network configuration has been changing over the years and a perfect geometry is not given due to visibility constraints that lead to subnetting in the network observations.

For the comparison in the time domain we used the intensive CONT94 campaign. The results of this comparison have been described in *Scherneck* and *Haas* [1999] and will only be summarized here briefly. We predicted VPMU variations for the CONT94 observations and compared the predictions to results from VLBI data analysis. For the analysis we estimated hourly polar motion and UT1 values once with vertical and horizontal ocean tide loading and once only with vertical ocean tide loading. The differences between the hourly PMU were compared to the predicted values.

The observed VPMU variations show typical tidal behavior in the semidiurnal and diurnal frequency bands and are similar to the predicted effects. The observed effects are larger than the predicted ones by a factor of 2–3 and appear to have a complicated frequency dependence since diurnal variations are less attenuated than semidiurnal ones. The reason for these discrepancies is most probably again as above, namely idealized conditions in the computation of the predictions.

5 Conclusions

This study shows the importance of horizontal ocean tide loading for the determination of polar motion and UT1 (PMU) with space geodetic techniques. A geodetic network consisting of a finite number of participating stations exhibits a common rotation mode due to horizontal ocean tide loading which is not negligible. Neglect of horizontal ocean tide loading in the analysis of space geodetic data contaminates the derived polar motion and UT1 values in form of small periodic rotations that have similar character as the influences coming from matter and motion perturbations in the ocean tide via rotation dynamics.

We predicted virtual PMU variations due to neglect of horizontal ocean tide loading in the frequency and the time domain and verified these predictions by analysis of geodetic VLBI data. Other space geodetic methods, e.g. GPS will be affected in the same way, of course.

Differences in existing ocean tide models have predicted effects on virtual PMU variations of up to 40 μas and 3 μsec for polar motion and UT1, respectively. They will be of importance for future earth rotation studies considering the expected accuracies of e.g. the CORE program. Today these tiny effects are still to small to be detected, but in the future they are likely to reach the detection threshold.

For the analysis of space geodetic data the best available ocean tide loading models should be used. Comparison of existing theoretical ocean tide loading models to empirical results from VLBI [e.g. *Sovers*, 1994, *Haas* and *Schuh*, 1998] and GPS are useful to verify and/or refine ocean tide loading models.

Acknowledgements. Figures in this paper were made with GMT software [*Wessels* and *Smith*, 1995]. This research has made use of NASA Goddard Space Flight Center's VLBI terrestrial reference frame solution number 1102g, 1998 August. Rüdiger Haas is supported by the European Union within the TMR programme under the contract FMRX-CT960071. This project is supported by grants from the Natural Science Research Council of Sweden under account G-AA/GU 03590.

References

Clark, T.A., C. Ma, J.W. Ryan, B.F. Chao, J.M. Gipson, D.S. MacMillan, N.R. Vandenberg, T.M. Eubanks and A.E. Niell, Earth Rotation Measurement Yields Valuable Information About the Dynamics of the Earth System, *EOS Trans., Amer. Geophys. U., Vol. 79*(17), 1998

Eanes, R.J., and S. Bettadpur, The CSR 3.0 global ocean tide model, *Technical Memorandum, CSR-TM-95-06*, Center for Space Research, 1995

Gipson, J.M., Very long baseline interferometry determination of neglected tidal terms in high-frequency Earth orientation variation, *J.Geophys.Res, 101*, 28051-28064, 1996

Greenberg, D.A., Modeling tidal power, *Sc. American 257:5*, 106–113, 1987

Haas, R. and H. Schuh, Ocean Loading Observed by Geodetic VLBI, *Proc. of the XIIIth Int. Symp. on Earth Tides, Brussels, July 1997*, Ducarme (ed.), 111-120, Observatoire Royal de Belgique, 1998

Le Provost, C., M.L. Genco, F. Lyard, P. Vincent, and P. Canceil, Spectroscopy of the world ocean tides from a finite element hydrodynamic model, *J. Geophys. Res., 99*, 24777-24797, 1994

Ma, C. and J.W. Ryan, NASA Space Geodesy Program – GSFC DATA Analysis – 1998, VLBI Geodetic Results 1979-1998, August, 1998

Ma, C., J.M. Sauber, L.J. Bell, T.A. Clark, D. Gordon, and W.E. Himwich, Measurement of horizontal motions in Alaska using very long baseline interferometry, *J. Geophys. Res., 95*, 21991-22011, 1990

Ray, R.D., D.J. Steinberg, B.F. Chao and D.E. Cartwright, Diurnal and Semidiurnal Variations in the Earth's Rotation Rate Induced by Oceanic Tides, *Science, 264*, 830-832, 1994

Scherneck, H.-G., A parameterized Solid Earth Tide Model and Ocean Tide Loading Effects for Global Geodetic Baseline Measurements, *Geophys. J. Int., 106*, 677-694, 1991

Scherneck, H.-G., A comprehensive and tentatively complete summary of oceanic effects in space geodetic baseline measurements, *Proceedings of the 11th Working Meeting on European VLBI for Geodesy and Astrometry*, G. Elgered (ed.), Research Report No 177, Onsala Space Observatory, Chalmers University of Technology, 121-133, 1996

Scherneck, H.-G. and R. Haas, Effect of horizontal displacements due to ocean tide loading on the determination of polar motion and UT1, *Geophys. Res. Lett., 26*, 501–504, 1999

Schwiderski, E.W., On charting global ocean tides, *Rev. Geophys. Space Phys. 18*, 243-268, 1980

Sovers, O.J., Vertical Ocean Loading Amplitudes from VLBI Measurements, *Geophys. Res. Lett., 21*, 357-360, 1994

Sovers, O.J., and C.S. Jacobs, Observation Model and Parameter Partials for the JPL VLBI Parameter Estimation Software "MODEST"-1996, *JPL Publication 83-39, Rev. 6*, JPL, 1996

Wessels, P., and W.H.F. Smith, Free software helps map and display data, *EOS Trans., Amer. Geophys. U., Vol. 55*, 293–305, 1991